RSC Advances

RSC Publishing

PAPER

View Article Online
View Journal | View Issue



Cite this: *RSC Adv.*, 2013, **3**, 22185

# A UV light enhanced $TiO_2$/graphene device for oxygen sensing at room temperature†

Jia Zhang,[ab] Chao Zhao,[b] Ping An Hu,*[a] Yong Qing Fu,*[b] Zhenlong Wang,*[a] Wenwu Cao,[c] Bin Yang[c] and Frank Placido[b]

Received 10th July 2013
Accepted 20th September 2013

DOI: 10.1039/c3ra43480j

www.rsc.org/advances

A room temperature oxygen sensor based on $TiO_2$/graphene device was developed with an enhanced sensing performance by UV light. A logarithmic relationship between the sensing response and $O_2$ concentration (from 134 ppm to 100%) was obtained. The sensor also shows an improved response and recovery with the durations of 193 s and 135 s at RT and atmosphere pressure, respectively. Herein, UV light was employed to excite electron–hole pairs in the $TiO_2$ film and the photogenerated electrons were scavenged by graphene and percolated to the collecting electrode, while the holes recombined with the electrons within $TiO_2$ film. This process will deplete the electron further thereby changing the conductivity of the device rapidly resulting in a much better sensing signal.

## 1. Introduction

Monitoring of oxygen gas ($O_2$) is critical in various fields, such as medicine, human safety, agriculture, military and environment monitoring. Conventional methods to detect the oxygen gas typically use potentiometric[1] and amperometric sensors.[2] However, their complex structures and bulky size limit their wide applications. In recent years, metal oxide semiconductors, such as CaO–$ZrO_2$, $Nb_2O_5$, $SrTiO_3$, ZnO, $In_2O_3$, and $SnO_2$, *etc.*, have been proven sensitive to oxygen content.[3] The conductivity of these metal oxide materials depends strongly on the amount of adsorbed $O_2$, which is commonly used as the sensing signal. Specially, titanium dioxide ($TiO_2$) is one of the most widely studied semiconductors for $O_2$ sensing applications,[4,5] owing to excellent physical and chemical stability, non-toxic, desirable electronic and optical properties and a low cost.[6] It is an n-type semiconductor for a wide range of $O_2$ sensing. Since the valence band (filled O-2p states) is nonreceptive to holes and the conduction band (Ti-3d states) is receptive to electrons, the conductivity is due to only the electrons in undoped $TiO_2$. Up to now, bulk, thin film and nanostructure of the $TiO_2$ have been developed to detect $O_2$.[7,8] However, some require high operating temperature (*e.g.* 300–1000 °C)[4] or high vacuum test conditions;[9] some exhibit slow response and recovery;[10] some suffer from the complicated fabrication techniques;[11] and others lack high sensitivity but a high-cost.[12]

Recently, hybrid of $TiO_2$ with nanoscale carbon materials have attracted significant attention. Many experimental efforts[13–15] and theoretical simulations[16–18] have been focused on the synthesis of hybrid $TiO_2$/graphene nanocomposites, where high stability and enhanced photovoltaic properties have been demonstrated. Graphene, a single layer atomic sheet of $sp^2$-bonded carbon atoms,[19] has been extensively researched in photovoltaic and photocatalysis hybrid materials owing to large specific surface area, ultrafast carries mobility, high thermal stability and excellent mechanical flexibility.[20] The $TiO_2$/graphene hybrid was demonstrated to be very fast and high efficient charge separation at the interface of the $TiO_2$/graphene,[16–18] which is widely used in photodetector, photocatalyst and solar cells. But for gas sensing, only Wang *et al.* reported the $TiO_2$-decorated graphene can be used as platform for $O_2$ sensing.[21] Further investigations are needed to develop new sensor structures and improve sensing performances.

To overcome the common drawbacks of the $TiO_2$-based oxygen sensor (high operated temperature, slow response and recovery rate and low sensitivity), herein, we propose a facile fabrication of a hybrid device as $O_2$ gas sensor by evaporating a thin amorphous $TiO_2$ film on the chemical vapor deposition grown graphene (CVD-graphene). The device showed a high sensitivity to $O_2$ with UV light when operated at room temperature. Sensitivity, stability, response and recovery time of the device were investigated at room temperature with UV light, and the sensing mechanism was discussed.

[a]*Key Lab of Microsystem and Microstructure, Harbin Institute of Technology, Ministry of Education, No. 2 YiKuang Street, Harbin, 150080, China. E-mail: hupa@hit.edu.cn; wangzl@hit.edu.cn*

[b]*Thin Film Centre, Scottish Universities Physics Alliance (SUPA), University of the West of Scotland, Paisley, PA1 2BE, UK. E-mail: richard.fu@uws.ac.uk*

[c]*Condensed Matter Science and Technology Institute, Harbin Institute of Technology, Harbin 150080, China*

† Electronic supplementary information (ESI) available. See DOI: 10.1039/c3ra43480j

## 2. Experimental details

### 2.1. Preparation of $TiO_2$/graphene device

Graphene was synthesized using chemical vapor deposition and then transferred to silicon substrate with a 300 nm thermal oxide layer.[22] In brief, the copper strips (Alfa Aesar, 99.95% purity) were loaded into fused silica tube and heated to 1035 °C under the $H_2$/Ar = 50/450 sccm (standard-state cubic centimeter per minute), followed by annealing for 20 min at the same temperature. Then, 1 sccm methane was introduced into the system for 20 min and then cooled to room temperature with the same gas. A PMMA supported transfer method was utilized to transfer graphene to the $SiO_2$/Si substrate for characterization and application. Then, a ~200 nm $TiO_2$ film was deposited directly on graphene film using electron beam evaporation.[23] Finally, sputtered Cr/Au (10/90 nm) electrodes were deposited on the graphene and $TiO_2$ film respectively to form a device. To improve the contact between metal electrodes and graphene or $TiO_2$ film, the devices were thermal annealed in $H_2$/Ar (10/20 sccm) atmosphere at 200 °C for 20 min. As contrast, pristine graphene based device and pure $TiO_2$ film based device were also fabricated and the $O_2$ sensing experiments were carried out at the same conditions.

### 2.2. Characterizations

The morphology of the $TiO_2$ was characterized using scanning electron microscopy (SEM, Hitachi SU-8000 with accelerating voltage of 15 kV). Optical image of the device was taken using an OLYMPUS BX41 microscope. Atomic force microscopy (AFM) images were acquired in the tapping mode with a commercial multimode Nanoscope IIIa (Veeco Co. Ltd). X-ray diffraction (XRD, Siemens D5000 Cu Kα, 40 kV/30 mA) was used to characterize the crystallinity of the $TiO_2$ film. Raman spectroscopy (HORIBA Jobin Yvon Co. Ltd) using a 532 nm laser with an incident power of 0.1 mW was used to characterize the uniformity, layer count and defect level of the graphene and deposited $TiO_2$ film.

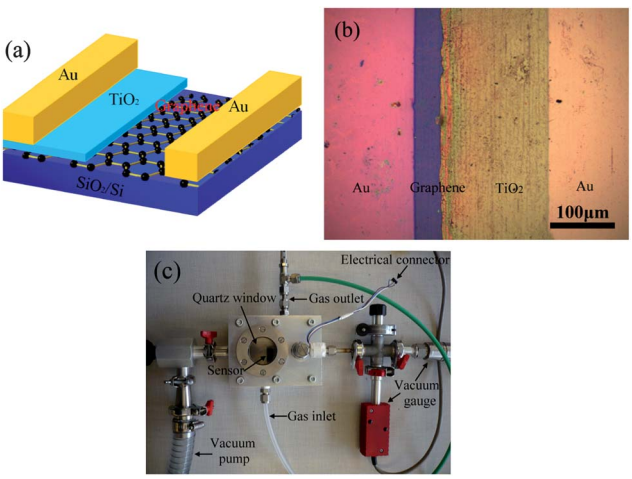


**Fig. 1** Characterization of the $TiO_2$/graphene device. (a) Schematic diagram of the device. (b) Optical image of the device, each part is denoted. (c) A home-made gas sensing setup for oxygen sensing measurements.

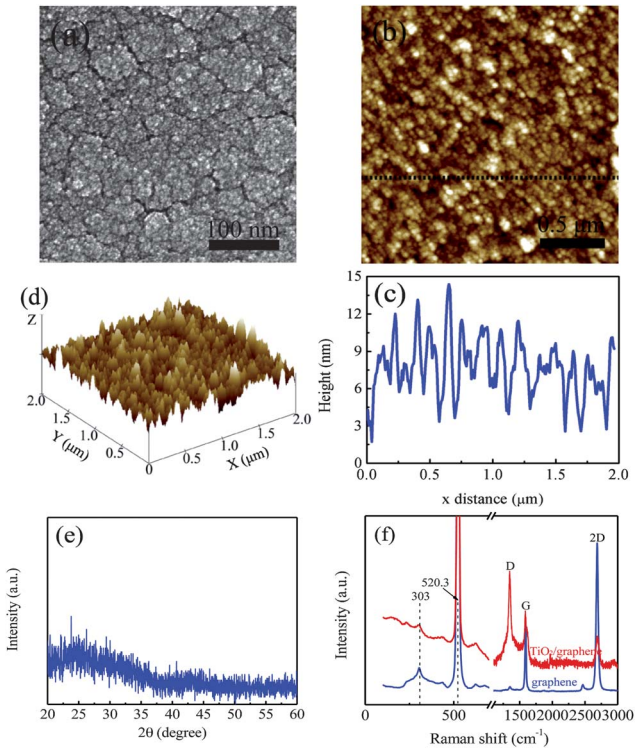


**Fig. 2** Characterizations of the as-deposited $TiO_2$ film. (a) SEM image of the $TiO_2$ film. (b) A top-view AFM image of the $TiO_2$ film. (c) Height profile of the line marked in (b). (d) A 3D-view AFM image of the $TiO_2$ film. (e) XRD pattern of the $TiO_2$ film, (f) Raman spectra of graphene film before and after $TiO_2$ film deposition.

### 2.3. Sensing measurements

The $O_2$ sensing measurements were carried out using a home-made setup as shown in Fig. 1c, which consists of a chamber with a quartz window for light irradiation, two channels for gas flow, and multiple connectors for electrical characterization. The base pressure was $1.0 \times 10^{-1}$ mbar with a mechanical pump. The $O_2$ concentration was controlled by a mass flow controller, which dilutes $O_2$ in $N_2$ at different volume ratios ($V_{O2}/(V_{O2} + V_{N2})$) in the chamber. Current–voltage ($I$–$V$) measurements were taken to characterize the sensing capability of the device and the electrical signal was recorded using a Keithley 2400. A UV lamp (with wavelength in range of 340–410 nm and an incident power density of ~0.83 mW $cm^{-2}$) was used for UV irradiation of the device through the quartz window. In addition, the temperature on the device surface was below 40 °C under the UV irradiation, measured using an infrared thermal camera. Therefore, the influence of thermo-effect on electrical properties of the device can be negligible.

## 3. Results and discussion

Fig. 1a illustrates the structure of the designed $TiO_2$/graphene hybrid device. Note that the $TiO_2$ film was deposited directly on

 

graphene and one of electrodes contacts completely with the $TiO_2$ film. Fig. 1b shows an optical image of the as-made $TiO_2$/graphene device and each part is denoted.

The SEM image (Fig. 2a) shows the morphology of the $TiO_2$ film, which is composed of nanoparticles, aggregations and clusters. These interconnected nanostructured $TiO_2$ form conductive channels and perform functions of a receptor and a transducer simultaneously.[24] Fig. 2b shows a top-view AFM image of the $TiO_2$ film, in which the $TiO_2$ nanostructured (nanoparticles, aggregations and clusters) are identified clearly. Height profile of the line marked in Fig. 2b is shown in Fig. 2c, which indicates as-deposited $TiO_2$ film is rough. This is one of critical factors on sensitivity and response time of the device. Previously results showed that nanoparticulate of metal oxides exhibited an increased sensitivity as well as a faster response and recovery rate compared with microcrystalline materials due to the larger surface-to-bulk ratio and porosity.[24–27] Fig. 2d shows a 3D-view AFM image of the $TiO_2$ film, from which the rough surface is identified further. The rough surface will be benefit for the gas absorption and reduce the reflection of incident light. As a consequence, we have fabricated an efficient $TiO_2$ nanostructure both for $O_2$ and UV light absorption.

Usually, the $TiO_2$ synthesized using methods such as hydrothermal, sol–gel, sputtering and evaporation, is amorphous before calcination.[28] This amorphous $TiO_2$ has larger specific surface area and more oxygen vacancies on the surface and in the bulk compared with that of crystalline $TiO_2$, which could provide higher carrier concentration and more active sites thereby enhance the interaction to oxygen gas.[29] Fig. 2e shows a typical XRD pattern of as-deposited $TiO_2$ film and no characteristic peak is observed indicating its amorphous nature (hereafter called $TiO_2$, except special informed). Furthermore, the crystallinity of the $TiO_2$ film is investigated by Raman spectroscopy and results are shown in Fig. 2f. Note that the peaks (at 303 $cm^{-1}$ and 520.3 $cm^{-1}$) in the range of 100–700 $cm^{-1}$ are assigned to $SiO_2$ substrate in the pristine graphene sample,[30] while the same peaks are observed in the $TiO_2$/graphene sample. Compared with the Raman spectra of the crystalline $TiO_2$,[31] the as-deposited $TiO_2$ is proven to be amorphous further. Herein, we used this amorphous $TiO_2$ thin film as sensitive element without further calcination. The higher content of oxygen vacancies will increase the concentration of electron thereby exhibiting of n-doping in $TiO_2$.

Furthermore, Fig. 2f also shows the Raman spectra collected from the pristine graphene and as-deposited $TiO_2$/graphene hybrid film. The G-band at ~1580 $cm^{-1}$ and 2D-band at ~2680 $cm^{-1}$ confirm the presence of graphitic carbon.[32] The D-band at ~1350 $cm^{-1}$ corresponds to the defect level. For the pristine graphene, the intensity ratio of 2D-band over G-band ($I_{2D}/I_G$) is about 2, with the full width at half-maximum (fwhm) of 2D-band of ~35 $cm^{-1}$, which confirms the appearance of single-layer graphene.[33] When the single-layer graphene is covered by $TiO_2$ thin film, the 2D band shifts from 2686 $cm^{-1}$ (pristine graphene) to 2672 $cm^{-1}$ ($TiO_2$/graphene), due to a Fermi level shift as a result of electron doping of graphene.[34] In addition, the fwhm value of the 2D band increases from ~35 $cm^{-1}$ (pristine graphene) to ~47 $cm^{-1}$ ($TiO_2$/graphene) and $I_{2D}/I_G$ decreases. The results are consistent with those observations in a typical electron doping of graphene.[34,35] Note that there is a remarkable increase in the intensity of D band compared with a negligible D band in the pristine graphene. This suggests that the electron doping occurs not only at the $TiO_2$/graphene interface but also in the graphene as a substitutional doping.[36]

Oxygen is active in forming electron traps after being adsorbed onto surfaces of many metal oxide.[37] Upon adsorption, the reaction of $O_2 + e^- \rightarrow O_2^-$ will occur when the temperature is below 420 K resulting in the formation of negatively charged ions on the surface. It is well known that surface defects on the materials (*e.g.* oxygen vacancies and adsorption sites) will promote the $O_2$ adsorption, causing the formation of more negatively charged ions ($O_2^-$, $O^-$, $O^{2-}$).[4] These chemisorbed ions deplete the surface electron states and result in the formation of an electron depletion layer, leading to the reduction of conductivity of the materials. In this study, UV irradiation was employed to excite electron–hole pairs in the $TiO_2$ film and the electron–hole pair was separated at the $TiO_2$/graphene interface. This will significantly change the conductance of sensing elements resulting in a much better sensing signal.

Fig. 3a shows a typical current–voltage (*I–V*) curve of the device measured in pure $N_2$ without UV light. A linear relationship of the applied voltage and current indicates an Ohmic contact between the electrode and graphene or $TiO_2$ film. It is different from the traditional device based on wide band gap semiconductors (*e.g.* ZnO, $TiO_2$), which shows typical Schottky or rectified contact.[38,39] In our experiments, there is a similar work function among the $TiO_2$ (4.2–4.4 eV),[40] graphene (4.5–4.8 eV)[41] and Cr/Au electrode (4.5–5.1),[40] which would reduce the Schottky barrier height between the semiconductor and contacted electrodes. In addition, the annealing process after deposited the Cr/Au electrodes will induce a metallization,[42] which is benefit to form an Ohmic contact. As a result, the as-made $TiO_2$/graphene hybrid device or pure $TiO_2$ film based device show linear *I–V* curves (Ohmic contact).

Furthermore, we have measured the *I–V* characteristics of the device in pure $N_2$ and $O_2$ with and without UV light, respectively. All tests are operated at room temperature and ambient pressure. Without UV light, there is only a minor change in the current measured in $O_2$ compared with that in $N_2$. The current of the device shows a slight decrease in the $O_2$ atmosphere, which can be explained by the reaction of

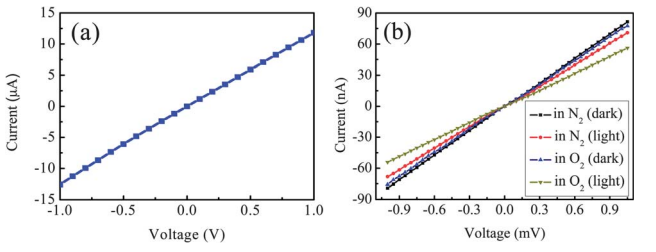


**Fig. 3** Current–voltage (*I–V*) characteristics of the $TiO_2$/graphene device measured at different sensing conditions. (a) *I–V* curve of the device in the pure $N_2$ without UV light (dark). (b) *I–V* curves of the device measured in $N_2$ and $O_2$ with and without UV light.

$O_2 + e^- \rightarrow O_2^-$ at RT.[37] Electrons are consumed by the newly absorbed $O_2$ molecules leading to an thicker electron-depleted surface region, which decreases the electron concentration in the device and thus decreases in conductivity. With UV light, photo-induced electrons and holes are separated at the interface of $TiO_2$ and graphene. Photogenerated electrons are scavenged fast by the graphene and percolate to the collecting gold electrode, while the photogenerated holes are recombination with the electrons within $TiO_2$ film. This process will deplete the electron further thereby decreasing the conductivity of the device. As a result, there is a nearly 40% decrease in the current, which is larger than previous $O_2$ sensor reported in ref. 21. The slight decrease of current in $N_2$ (15.3%) with UV light may be attributed to residual oxygen in the chamber considering the base pressure is $1.0 \times 10^{-1}$ mbar. To confirm the change in the $N_2$ atmosphere, the device was placed in a high vacuum chamber (Lakeshore probe station, Desert Cryogenics Co. Ltd) and the a higher vacuum of $5.0 \times 10^{-5}$ mbar was achieved after pumping for 12 h to remove the residual oxygen and then backfilled with high purity nitrogen (99.99%). The resistance of the device changes by ~8.1% with and without the UV light (Fig. S1†). Therefore, we attribute the change of the device to the residual oxygen in the chamber considering the different base pressures. The apparent change in the current readings in $O_2$ over those in $N_2$ clearly indicates that UV light improves the sensitivity of the device for $O_2$ sensing. In contrast, we have measured the *I–V* curves of the pristine graphene device and $TiO_2$ device in $O_2$ with and without UV light (Fig. S2c and d†). Both of the devices show a negligible current change indicating these materials or structures are not sensitive to oxygen.

Fig. 4a shows representative single sensing cycle of the device exposure to $O_2$ at RT with UV light. Resistance increases in the presence of $O_2$ and recovers in $N_2$. The sensing response signal ($S$) of the device is defined as: $S = (R - R_0)/R_0 \times 100\%$, where $R_0$ and $R$ are the resistance values measured in pure $N_2$ and different concentrations of $O_2$ with UV light. The response time and recovery time, defined as the time needed to achieve 90% of the final equilibrium value,[43] are estimated to be 193 s and 135 s, respectively. Note that the recovery process, corresponding to desorption of gas molecules, is usually speeded up using heating or UV irradiation, which can achieve fast and complete recovery.[44–46] Thus, the UV light would not only improve the sensitivity of the device for $O_2$, but also reduce the recovery time. Many researchers have developed the nanostructured $TiO_2$-based $O_2$ sensor but failed to achieve fast response and recovery process. Lu *et al.*[47] demonstrated there was a negligible change in conductivity of $TiO_2$ thin film based $O_2$ sensor while operated at 31 °C, even at elevating $O_2$ concentrations. Llobet *et al.*[48] optimized the sintered time and operated temperature resulting in response and recovery durations of 1.5–3.0 min and 7.0–6.0 min, respectively. Cheng *et al.*[49] used amorphous $TiO_2$ nanotube arrays for $O_2$ sensing and the response time was estimated to be several minutes. Wang *et al.* demonstrated a fast response rate (~130 s), but a slower recovery rate (~260 s).[21] By comparison, our results show a significant improvement in response and recovery time for $O_2$ detection operated at RT.

Fig. 4b shows the time response of $S$, when sequentially exposed to $N_2$ and various concentration of $O_2$ with UV light. Clearly, the response readings increases as $O_2$ concentration and achieve saturation within the given duration as $O_2$ concentration above 1% here. Fig. 4c shows the relationship between the sensing signal and the $O_2$ concentration, which is logarithmic in large concentration range of 0.0134% to 100%. It can be fitted by:

$$S = 5.17 \lg X + 26.23 \quad (1)$$

where, $X$ is the $O_2$ concentration (%). This newly developed device is able to give quantitative values for practical $O_2$ sensing applications. The $O_2$ concentration can be determined by the formula $X = 10^{[(S-26.23)/5.17]}$ with the measured sensing signal. The larger linear scope compared with that in ref. 21, suggests that as-made sensor is readily to detect the trace of $O_2$ and practicality. The $O_2$ detection limit is as low as ~134 ppm for the prepared device similar to previous result,[21] and of course, the detection limit may be further lowered by optimizing the device. The stability of the sensor is measured by sequentially exposed to $N_2$ and $O_2$ with UV light showing in Fig. 4d (black curve). The conductivity can be nearly recovered. Otherwise, a little increasing base line is normal in the gas sensing owing to the residual gas in the chamber. However, the pristine graphene devices don't show any clear response to $O_2$ at the same conditions (Fig. 4d red curve). Further, the response of the pristine graphene device and $TiO_2$ device sequent exposure to $N_2$ and $O_2$ with UV light (Fig. S2e and f†) shows a small change of the sensing response signal with <1.5% and <4.5% for the pristine graphene device and $TiO_2$ device, respectively.

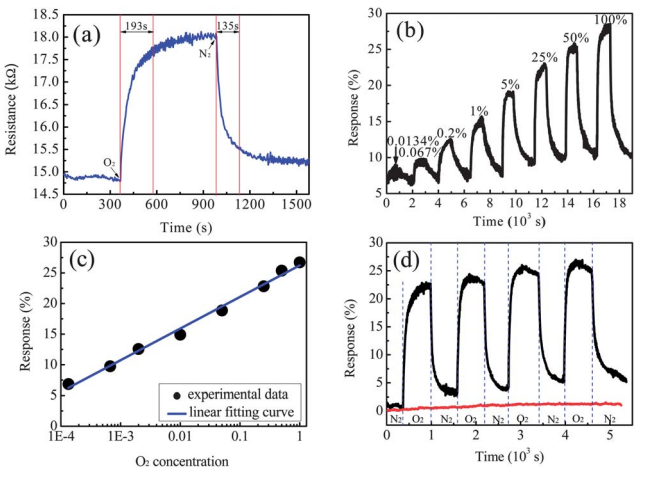


**Fig. 4** Oxygen sensing using $TiO_2$/graphene device. (a) Single sensing cycle for $O_2$ with UV light at room temperature, $V_{bias} = 1$ mV. (b) Response of the device to different $O_2$ concentrations, $V_{bias} = 1$ mV. (c) Response with respect to $O_2$ concentrations (logarithmic concentration). (d) Typical sensing cycles of the device exposure to $N_2$ and $O_2$ in sequence with UV light, $V_{bias} = 1$ mV.

## 4. Conclusion

In summary, a reliable and scalable oxygen sensor based on $TiO_2$/graphene hybrid device has been developed and shown

 

enhanced performance with UV light. This sensor exhibits highly sensitive to $O_2$ at RT with detect limitation of 134 ppm. In addition, a logarithmic relationship between sensing response signal ($S$) with $O_2$ gas concentration has been demonstrated in the huge concentration range of 134 ppm ~100%. The sensor also shows an improved response and recovery with the durations of 193 s and 135 s at RT and atmosphere pressure, respectively.

## Acknowledgements

This work is supported by the National key Basic Research Program of China (973 Program) under Grant no. 2013CB632900, National Natural Science Foundation of China (NSFC, no. 61172001), Scottish Sensing Systems Centre (S3C), Carnegie Trust Funding, Royal Society of Edinburgh, UK; the Scientific Research Foundation for the Returned Overseas Chinese Scholars, State Education Ministry and the Fundamental Research Funds for Central Universities, Chinese Program for New Century Excellent Talents in University and Doctoral Visiting Scholar Program of Harbin Institute of Technology.

## References

1 N. Yamazoe and N. Miura, *IEEE Trans. Compon., Packag., Manuf. Technol., Part A*, 1995, **18**, 252.
2 W. Weppner, *Mater. Sci. Eng., B*, 1992, **15**, 48.
3 E. Kanazawa, G. Sakai, K. Shimanoe, Y. Kanmura, Y. Teraoka, N. Miura and N. Yamazoe, *Sens. Actuators, B*, 2001, **77**, 72.
4 R. Ramamoorthy, P. K. Dutta and S. A. Akbar, *J. Mater. Sci.*, 2003, **38**, 4271.
5 D. P. Macwan, P. N. Dave and S. Chaturvedi, *J. Mater. Sci.*, 2011, **46**, 3669.
6 U. Diebold, *Appl. Phys. A: Mater. Sci. Process.*, 2002, **76**, 1.
7 M. E. Franke, T. J. Koplin and U. Simon, *Small*, 2006, **2**, 36.
8 R. A. Potyrailo, C. Surman, N. Nagraj and A. Burns, *Chem. Rev.*, 2011, **111**, 7315.
9 J. J. Pireaux, M. Chtaïb, J. P. Delrue, P. A. Thiry, M. Liehr and R. Caudano, *Surf. Sci.*, 1984, **141**, 211.
10 C.-C. Lu, Y.-S. Huang, J.-W. Huang, C.-K. Chang and S.-P. Wu, *Sensors*, 2010, **10**, 670.
11 E. I. Tiffee, K. H. Hardtl, W. Menesklou and J. Riegel, *Electrochim. Acta*, 2001, **47**, 807.
12 M. Mogensen, N. M. Sammes and G. A. Tompsett, *Solid State Ionics*, 2000, **129**, 63.
13 H. Y. Gao, W. Chen, J. Yuan, Z. Jiang, G. X. Hu, W. F. Shangguan, Y. Z. Sun and J. C. Su, *RSC Adv.*, 2013, **3**, 8559.
14 X. J. Liu, L. K. Pan, T. Lv, G. Zhu, T. Lu, Z. Sun and C. Q. Sun, *RSC Adv.*, 2011, **1**, 1245.
15 J.-H. Yun, R. J. Wong, Y. H. Ng, A. J. Di and R. Amal, *RSC Adv.*, 2012, **2**, 8164.
16 A. J. Di, Y. H. Ng, N. J. Bell, Z. H. Zhu, R. Amal and S. C. Smith, *J. Phys. Chem. Lett.*, 2011, **2**, 894.
17 K. K. Manga, Y. Zhu, Y. L. Yan and K. P. Loh, *Adv. Funct. Mater.*, 2009, **19**, 3638.
18 R. Long, N. J. English and O. V. Prezhdo, *J. Am. Chem. Soc.*, 2012, **134**, 14238.
19 K. S. Novoselov, A. K. Geim, S. V. Morozov, D. Jiang, Y. Zhang, S. V. Dubonos, I. V. Grigorieva and A. A. Firsov, *Science*, 2004, **306**, 666.
20 V. Singh, D. Joung, L. Zhai, S. Das, S. I. Khondaker and S. Seal, *Prog. Mater. Sci.*, 2011, **56**, 1178.
21 Q. Wang, X. F. Guo, L. C. Cai, Y. Cao, L. Gan, S. Liu, Z. X. Wang, H. T. Zhang and L. D. Li, *Chem. Sci.*, 2011, **2**, 1860.
22 J. Zhang, P. A. Hu, X. N. Wang, Z. L. Wang, D. Q. Liu, B. Yang and W. W. Cao, *J. Mater. Chem.*, 2012, **22**, 18283.
23 Ö. Duyar, F. Placido and H. Z. Durusoy, *J. Phys. D: Appl. Phys.*, 2008, **41**, 095307.
24 N. Yamazoc, G. Sakai and K. Shimanoe, *Catal. Surv. Asia*, 2003, **7**, 63.
25 C. Xu, J. Tamaki, N. Miura and N. Yamazoe, *Sens. Actuators, B*, 1991, **3**, 147.
26 F. Lu, Y. Li, M. Dong and X. Wang, *Sens. Actuators, B*, 2000, **66**, 225.
27 Z. A. Ansari, S. G. Ansari, T. Ko and J.-H. Oh, *Sens. Actuators, B*, 2002, **87**, 105.
28 X. B. Chen and S. S. Mao, *Chem. Rev.*, 2007, **107**, 2891.
29 O. K. Varghese, D. W. Gong, M. Paulose, K. G. Ong and C. A. Grimes, *Sens. Actuators, B*, 2003, **93**, 338.
30 P. A. Temple and C. E. Hathaway, *Phys. Rev. B: Solid State*, 1973, **7**, 3685.
31 T. Ohsaka, F. Izumi and Y. Fujiki, *J. Raman Spectrosc.*, 1978, **7**, 321.
32 Y. F. Hao, Y. Y. Wang, L. Wang, Z. H. Ni, Z. Q. Wang, R. Wang, C. K. Koo, Z. X. Shen and J. T. L. Thong, *Small*, 2010, **6**, 195.
33 A. C. Ferrari, J. C. Meyer, V. Scardaci, C. Casiraghi, M. Lazzeri, F. Mauri, S. Piscanec, D. Jiang, K. S. Novoselov, S. Roth and A. K. Geim, *Phys. Rev. Lett.*, 2006, **97**, 187401.
34 A. Das, S. Pisana, B. Chakraborty, S. Piscanec, S. K. Saha, U. V. Waghmare, K. S. Novoselov, H. R. Krishnamurthy, A. K. Geim, A. C. Ferrari and A. K. Sood, *Nat. Nanotechnol.*, 2008, **3**, 210.
35 O. Frank, M. Mohr, J. Maultzsch, C. Thomsen, I. Riaz, R. Jalil, K. S. Novoselov, G. Tsoukleri, J. Parthenios, K. Papagelis, L. Kavan and C. Galiotis, *ACS Nano*, 2011, **5**, 2231.
36 J. M. Englert, C. Dotzer, G. Yang, M. Schmid, C. Papp, J. M. Gottfried, H.-P. Steinrück, E. Spiecker, F. Hauke and A. Hirsch, *Nat. Chem.*, 2011, **3**, 279.
37 C. X. Wang, L. W. Yin, L. Y. Zhang, D. Xiang and R. Gao, *Sensors*, 2010, **10**, 2088.
38 S. Liang, H. Sheng, Y. Liu, Z. Huo, Y. Lu and H. Shen, *J. Cryst. Growth*, 2001, **225**, 110.
39 L. A. Harris, *J. Electrochem. Soc.*, 1980, **127**, 2657.
40 N. Fuke, A. Fukui, A. Islam, R. Komiya, R. Yamanaka, H. Harima and L. Han, *Sol. Energy Mater. Sol. Cells*, 2009, **93**, 720.
41 Y.-J. Yu, Y. Zhao, S. Ryu, L. E. Brus, K. S. Kim and P. Kim, *Nano Lett.*, 2009, **9**, 3430.

42 H. K. Kim, S. H. Han, T. Y. Seong and W. K. Choi, *Appl. Phys. Lett.*, 2000, **77**, 1647.
43 M. R. Hoffmann, S. T. Martin, W. Y. Choi and D. W. Bahnemann, *Chem. Rev.*, 1995, **95**, 69.
44 A. Vertes and R. Gijbels, *Rapid Commun. Mass Spectrom.*, 1990, **4**, 228.
45 I. P. Herman, *Chem. Rev.*, 1989, **89**, 1323.
46 Y. Yanagisawa and Y. Ota, *Surf. Sci.*, 1991, **254**, 433.
47 C.-C. Lu, Y.-S. Huang, J.-W. Huang, C.-K. Chang and S.-P. Wu, *Sensors*, 2010, **10**, 670.
48 E. Llobet, E. H. Espinosa, E. Sotter, R. Ionescu, X. Vilanova, J. Torres, A. Felten, J. J. Pireaux, X. Ke, G. V. Tendeloo, F. Renaux, Y. Paint, M. Hecq and C. Bittencourt, *Nanotechnology*, 2008, **19**, 375501.
49 H. F. Lu, F. Li, G. Liu, Z.-G. Chen, D.-W. Wang, H.-T. Fang, G. Q. Lu, Z. H. Jiang and H.-M. Cheng, *Nanotechnology*, 2008, **19**, 405504.

 